The Raf-like Kinase *ILK1* and the High Affinity K^+ Transporter *HAK5* Are Required for Innate Immunity and Abiotic Stress Response[1][OPEN]

Elizabeth K. Brauer[2], Nagib Ahsan[3], Renee Dale, Naohiro Kato, Alison E. Coluccio, Miguel A. Piñeros, Leon V. Kochian, Jay J. Thelen, and Sorina C. Popescu[4]*

The Boyce Thompson Institute for Plant Research, Ithaca, New York 14853 (E.K.B., S.C.P.); Department of Plant Pathology and Plant-Microbe Biology, Cornell University, Ithaca, New York 14853 (E.K.B., S.C.P.); Department of Biochemistry, University of Missouri, Christopher S. Bond Life Sciences Center, Columbia, Missouri 65211 (N.A., J.T.T.); Department of Biological Sciences, Louisiana State University, Baton Rouge, Louisiana 70803 (R.D., N.K.); and Robert W. Holley Center for Agriculture and Health, Agricultural Research Service, US Department of Agriculture, Cornell University, Ithaca, New York 14853 (A.E.C., M.A.P., L.V.K.)

ORCID IDs: 0000-0002-1674-1247 (R.D.); 0000-0002-7166-1848 (M.A.P.); 0000-0003-3416-089X (L.V.K.); 0000-0001-5780-8252 (S.C.P.).

Plant perception of pathogen-associated molecular patterns (PAMPs) and other environmental stresses trigger transient ion fluxes at the plasma membrane. Apart from the role of Ca^{2+} uptake in signaling, the regulation and significance of PAMP-induced ion fluxes in immunity remain unknown. We characterized the functions of *INTEGRIN-LINKED KINASE1* (*ILK1*) that encodes a Raf-like MAP2K kinase with functions insufficiently understood in plants. Analysis of *ILK1* mutants impaired in the expression or kinase activity revealed that *ILK1* contributes to plant defense to bacterial pathogens, osmotic stress sensitivity, and cellular responses and total ion accumulation in the plant upon treatment with a bacterial-derived PAMP, flg22. The calmodulin-like protein CML9, a negative modulator of flg22-triggered immunity, interacted with, and suppressed ILK1 kinase activity. ILK1 interacted with and promoted the accumulation of HAK5, a putative $(H^+)/K^+$ symporter that mediates a high-affinity uptake during K^+ deficiency. *ILK1* or *HAK5* expression was required for several flg22 responses including gene induction, growth arrest, and plasma membrane depolarization. Furthermore, flg22 treatment induced a rapid K^+ efflux at both the plant and cellular levels in wild type, while mutants with impaired *ILK1* or *HAK5* expression exhibited a comparatively increased K^+ loss. Taken together, our results position *ILK*1 as a link between plant defense pathways and K^+ homeostasis.

During infection, bacteria betray their presence in the host through pathogen-associated molecular patterns (PAMPs), which are detected by pattern recognition receptors at the plasma membrane (PM). One of the best-characterized pattern recognition receptors is FLS2, which binds the flg22 peptide derived from bacterial flagellin (Gómez-Gómez and Boller, 2000; Chinchilla et al., 2007). Recognition of flg22 in Arabidopsis elicits signaling responses within minutes, including the initiation of kinase cascades, production of reactive oxygen species (ROS), and extracellular alkalization. A set of significant cellular responses triggered rapidly after stress perception involves the fluxes of cations and anions across the PM (Boller and Felix, 2009).

While certain ion-mediated signaling events and their contribution to defense responses are clear, others remain relatively unstudied. For example, Ca^{2+} influx was shown to activate anion efflux, ROS production, and Ca^{2+}-dependent protein kinase cascades, leading to changes in gene expression (Boudsocq et al., 2010; Jeworutzki et al., 2010, Kuchitsu et al., 1997; Felle et al., 1998; Wendehenne et al., 2002). In contrast, the role of K^+ and Cl^- efflux is largely unknown, although some evidence suggests that these fluxes contribute to intracellular signaling and immunity (Davies, 1987; Jeworutzki et al., 2010). Anion fluxes (Cl^- and NO_3^-) promote flg22-induced PM depolarization and are also required for PAMP-induced changes in gene expression and production of defensive compounds

[1] This work was supported by a post-graduate fellowship to E.K.B. from the National Science and Engineering Research Council of Canada, and by the National Science Foundation under project grants no. IOS-1025642 to S.C.P. and no. DBI-0604439 to J.J.T.

[2] Present address: Eastern Cereal and Oilseed Research Center, Agriculture and Agri-Food Canada, K1A 0C6, Ottawa, Canada.

[3] Present address: Division of Biology and Medicine, Brown University, Center for Cancer Research and Development, Proteomics Core Facility, Rhode Island Hospital, Providence, RI 02903.

[4] Present address: Department of Biochemistry, Molecular Biology, Entomology and Plant Pathology, Mississippi State University, Mississippi State, MS 39759.

* Address correspondence to scp319@msstate.edu.

The author responsible for distribution of materials integral to the findings presented in this article in accordance with the policy described in the Instructions for Authors (www.plantphysiol.org) is: Sorina C. Popescu (scp319@msstate.edu).

The study was conceived by E.K.B. and S.C.P. and work carried out by E.K.B., with the exception of the mass spectrometry assays (N.A., J.J.T.), the SLCA assays (R.D., N.K.), and *Xenopus* oocyte experiments (A.C., M.P., and L.V.K.); and the manuscript was written by E.K.B. and S.C.P., and reviewed by all authors.

[OPEN] Articles can be viewed without a subscription.

www.plantphysiol.org/cgi/doi/10.1104/pp.16.00035

in parsley (Jeworutzki et al., 2010; Jabs et al., 1997). Whether these non-Ca^{2+} ion fluxes have a direct or indirect effect on signaling during immunity remains unknown, in part because the molecular components involved in these processes have not yet been identified.

The mechanisms of ion transport, cross talk among ion transport systems, and regulatory pathways for maintaining ion homeostasis have been studied extensively in the context of plant nutrition. For example, under limiting K^+ conditions (10–200 μM external K^+), K^+ uptake is mediated by the high-affinity *HAK5* transporter and low-affinity *AKT1* channel in Arabidopsis (Spalding et al., 1999; Alemán et al., 2011). The regulation of both of these transport systems is responsive to the nutrient status of the extracellular environment. As such, conditions of K^+, N, or P deficiency induce *HAK5* expression while K^+ provision represses its expression (Rubio et al., 2014). HAK5 localization also changes in response to K^+ status, as deficiency enhances HAK5 accumulation at the PM (Qi et al., 2008). HAK5 transport activity, however, is specifically induced by K^+ deficiency through unknown posttranslational modifications (Rubio et al., 2014). In *Dionaea muscipula*, *DmHAK5* mediated K^+ uptake in *Xenopus* oocytes but only when co-expressed with the Ca^{2+}-induced AtCBL9-CIPK23 complex (Scherzer et al., 2015), suggesting that the transport activity is regulated by Ca^{2+} signals. CBL1 and CIPK23 were also found to enhance AtHAK5 transport in yeast and Arabidopsis (Ragel et al., 2015). Thus, K^+ deficiency promotes *HAK5* regulation at multiple levels and modifies K^+ uptake according to plant needs. Given that PAMP induced loss of anions, K^+, and other nutrients have the potential to promote bacterial growth in the apoplast, regulation of nutrient loss by the plant host is likely a critical aspect of PAMP-triggered immunity (Atkinson and Baker, 1987). Indeed, the pathways for maintaining nutrient homeostasis under abiotic stress may also mediate signaling and cellular responses after pathogen attack.

In an effort to identify components of the immune response that may be involved in modulation of ion transport, we characterized the Arabidopsis *INTEGRIN-LINKED KINASE1* (*ILK1*) that was previously called *ANKYRIN-PROTEIN KINASE 1* (Chinchilla et al., 2003). *ILK1* belongs to the *ILK* subfamily of RAF-like MAPKKKs that are ubiquitous across eukaryotes and the plant kingdom (Ichimura et al., 2002). In metazoans, *ILK*s have a central role in cellular motility; extracellular matrix signals perceived by the integrin transmembrane receptor are transmitted to numerous cytosolic signaling pathways through ILK (Wickström et al., 2010). In plants, *ILK* expression has been associated with changes in root development. The expression of *MsILK* in *Medicago sativa* was induced during nodule development while in Arabidopsis, expression of a mutated *ILK1* was associated with lateral root formation (Chinchilla et al., 2003, 2008). We previously identified *ILK1* as a *CML9* protein interactor, which has been shown to promote both flg22 responses and tolerance to high NaCl and KCl (Popescu et al., 2007; Magnan et al., 2008; Leba et al., 2012a; 2012b). Based on the role of *ILK*s in metazoans and of the plant *CML9* in abiotic and biotic stress, we hypothesized that *ILK1* may also be involved in environmental stress responses.

In this study, we demonstrate that *ILK1* promotes osmotic stress sensitivity, flg22 responses, and resistance to bacterial pathogens. ILK1 is an active kinase in vitro and ILK1 kinase activity is required for its roles in immunity, but not in osmotic stress. Protein interaction screens revealed that ILK1 interacts with the HAK5 K^+ transporter and induces its accumulation in the plant. Interestingly, *HAK5* and *ILK1* promote both growth in a limiting K^+ environment and flg22-induced responses. Furthermore, K^+ transport is required for flg22-induced PM depolarization and flg22-induced growth suppression. Together, these results suggest that K^+ transport mediated by *HAK5* and *ILK1* influences an important subset of immune and stress responses.

RESULTS

ILK1 Interacts with CML9 in Vivo and Is an Active Kinase

The calmodulin-like protein, CML9, interacts in vitro with a number of kinases including ILK1 (Popescu et al., 2007). To determine if ILK1 interacts with CML9 in vivo, the split-luciferase complementation assay (SLCA) was conducted in Arabidopsis protoplasts. Coexpression of *NLuc-ILK1* and *CLuc-CML9* produced significant luciferase activity relative to the negative control indicating interaction (Fig. 1A). No luciferase activity was observed during coexpression of *NLuc-ILK1* with *CLuc-CaM1*, a calmodulin that shares several common interactors with CML9 (Popescu et al., 2007), indicating specificity of the ILK1-CML9 interaction. To further evaluate whether ILK1 and CML9 interact in the absence of other plant proteins, the full-length *ILK1* and *CML9* genes were fused with complementary fragments of YFP and expressed in *Xenopus* oocytes to test for bimolecular fluorescence complementation. Coinjection of cRNA encoding *ILK1* and *CML9* resulted in a significant YFP signal, indicating a direct interaction of the protein products (Fig. 1B).

Several members of the ILK family, including ILK1, are classified as pseudokinases because they contain substitutions in conserved amino-acid motifs that are essential for enzymatic activity (Adams, 2001). In general, plant ILKs have fewer substitutions in the kinase domain compared to metazoan ILKs, suggesting that they may be functional kinases (Fig. 1C). The MsILK1 has an unusual Mn^{2+}-dependent kinase activity (Chinchilla et al., 2008), indicating that at least some plant ILKs are active. To test ILK1 kinase activity, a radioactive kinase assay was performed with purified recombinant ILK1-cMyc. The 75-kD ILK1-cMyc exhibited both autophosphorylation and substrate phosphorylation activity in the presence of either Mn^{2+} or Mg^{2+} cofactors (Fig. 1D). ILK1-dependent phosphorylation demonstrated a dose-dependent relationship with Mn^{2+} that was absent with Mg^{2+} (Fig. 1D). Consistent with this

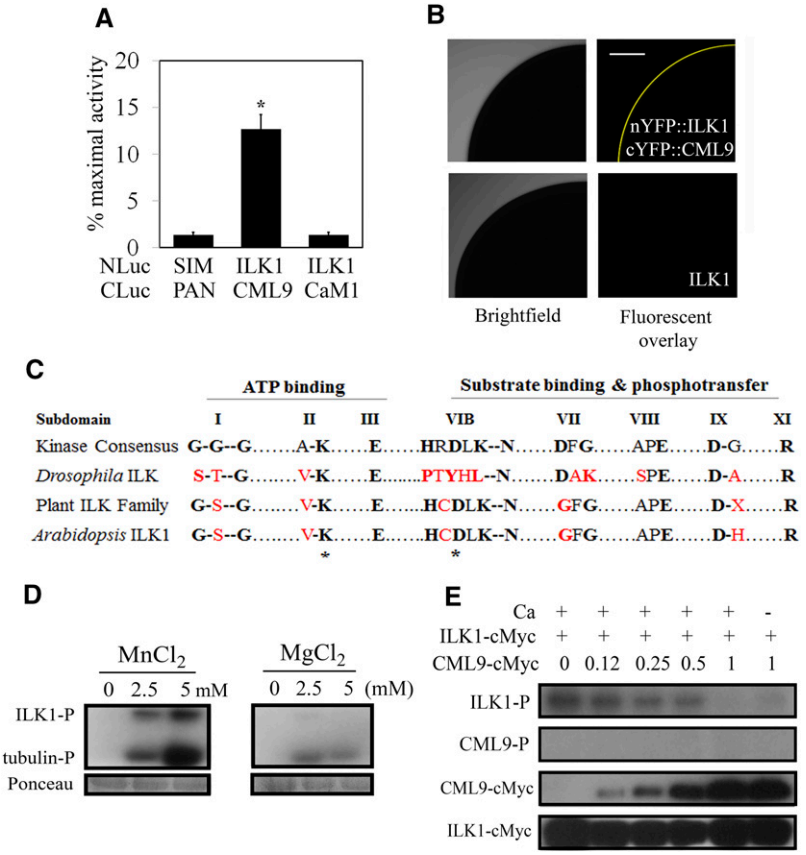

Figure 1. ILK1 interacts with CML9 in vivo and is an active kinase in vitro. A, The SLCA in Arabidopsis protoplasts revealed interactions between the bait (NLuc-ILK1) and prey (CLuc-CML9) fusion proteins by quantifying the amount of luciferase activity relative to that of the HISTONE 2A and 2B interactors (NLuc-H2A, CLuc-H2B; Fujikawa and Kato, 2007). The response of the negative control (NLuc-SIM, CLuc-PAN) is shown for reference. Data from four replicates from three independent experiments for each pair are shown where * indicates significant difference from the control, $P < 0.05$). B, Images showing interaction of ILK1 with CML9 by bimolecular fluorescence complementation of YFP in *Xenopus* oocytes. Scanning confocal microscopy images shows one-quarter of the oocyte either fluorescing (right image) or under bright field (left image). No background autofluorescence was observed in cells expressing untagged ILK1 ($n = 6$). C, The kinase domain of *ILK*s lacks several critical residues present in eukaryotic protein kinases. Alignment of the highly conserved amino acids within the kinase subdomains of the plant *ILK* family revealed higher conservation of kinase consensus residues in plants (black letters) compared to a representative metazoan *ILK* from *Drosophila*, which contains several substitutions (red letters). Asterisks indicate the residues mutated in this study. D, Autophosphorylation (ILK-P) and substrate phosphorylation (tubulin-P) of purified ILK1-cMyc with increasing concentrations of Mn^{2+} or Mg^{2+} cofactor visualized by autoradiography. Equal loading was determined by Ponceau staining. E, Autophosphorylation (ILK-P) and CML9 phosphorylation (CML9-P) with 5 mM Mn and 1 mM Ca, in the presence of increasing amounts of CML9-cMyc. Protein loading is visualized by western blot with an anticMyc antibody.

finding, two autophosphorylation sites near the N terminus (Ser-17 and Ser-26) were identified when ILK1-cMyc was exposed to Mn^{2+}, while only one site (Ser-17) was phosphorylated in the presence of Mg^{2+} (Supplemental Fig. S1; Supplemental Table S1). Mass spectrometry analysis of the purified ILK1-cMyc did not detect additional 75 kD kinases, and phosphorylation signals were absent in the empty vector control extracts (Supplemental Fig. S2, A and B). Together, these observations indicate that the signal was not due to contaminating plant kinases extracted during the purification process but rather represents ILK1-cMyc activity.

Next, we tested whether CML9 is an ILK1 substrate or is able to modulate ILK1 activity, by co-incubating purified CML9 and ILK1 fusion proteins. No CML9 phosphorylation was observed, indicating that CML9 is not an ILK1 direct phosphorylation target (Fig. 1E). Instead, ILK1 autophosphorylation diminished with increasing CML9 amounts in both the presence and absence of Ca^{2+}, suggesting that CML9 represses ILK1 activity regardless of Ca^{2+} presence.

ILK1 Functions as a Kinase during Flagellin Response and Basal Immunity

Ectopic expression of *CML9* is associated with root growth inhibition in response to flg22 (Leba et al.,

2012b). To determine if *ILK1* is similarly involved in responses to flg22, two independent mutant lines with T-DNA insertions in the promoter region (*ilk1-1*) or an exon (*ilk1-2*) were tested for *ILK1* expression, and found to have a significant reduction in *ILK1* transcript abundance (Fig. 2A; Supplemental Table S2). We challenged seedlings from these with flg22 and root growth was compared to the wild-type line 10 d after exposure. While flg22 significantly inhibited wild-type root growth relative to control conditions, *ilk1-1* or *ilk1-2* seedlings grew similarly in control or flg22-supplemented medium, indicative of a lower flg22 sensitivity that the wild type (Fig. 2B). Due to the similarity in response between *ilk1-1* or *ilk1-2* seedlings, subsequent experiments were performed with the *ilk1-1* line alone.

To determine if ILK1 activity is required for flg22 sensitivity, mutant ILK1 isoforms were generated with decreased ($ILK1^{K222A}$) and increased ($ILK1^{D319N}$) kinase activity (Fig. 3A). The three ILK1 isoforms were ectopically expressed in the *ilk1-1* background to restore ILK1 expression (Fig. 3B). Two independent transformants from each event were tested for root growth responses to flg22. Interestingly, while all of the lines expressing the kinase-active ILK1 isoforms (ILK1-1, ILK1-2, D319N-1, D319N-2) displayed significant flg22-induced root growth inhibition, the lines expressing the kinase-dead version (K222A-1, K222A-2) did not ($P = 0.19$, $P = 0.32$; Fig. 3C). All lines grew the same as wild type in control conditions, indicating that this phenotype cannot be explained by stunted growth of the transformants. This suggests that *ILK1* expression and activity are both required for flg22 sensitivity in seedlings.

Detection of flagellin is an important component of basal immunity against bacterial pathogens (Zipfel et al., 2004). To determine if basal immunity is affected by *ILK1*, *ilk1-1* plants were infected alongside wild-type and ILK1-1, K222A-1, and D319N-1 lines with the *Pseudomonas syringae* pv. *tomato* Δ*hrcQ-U* bacterial pathogen. This pathogen lacks a functional type-three secretion system and is unable to secrete effectors into the plant cell to disrupt PAMP detection. In line with the trend observed with flg22 treatment, the *ilk1-1* and K222A-1 plants were more susceptible to the pathogen while the other lines maintained wild-type-level resistance (Fig. 3D). This role is not likely related to stomatal aperture as susceptibility to a bacterial pathogen occurred during either flood-inoculation or direct infiltration (Supplemental Fig. S3). This suggests that ILK1 functions as a kinase in promoting resistance to bacterial pathogens. In contrast, the *ilk1-1* mutant performed like wild type when infected with the virulent strain (DC3000) or the avirulent *P. syringae* pv. *tomato* strain (DC3000 avrRpt2) indicating that *ILK1* is not involved in effector-induced defenses (Supplemental Fig. S3).

We next examined *ILK1* contribution to several early PAMP responses. To begin, *ilk1-1* leaf disks were exposed to flg22 followed by ROS quantification; no significant difference was observed between the *ilk1-1* and wild-type plants (Fig. 4A). Plant perception of flg22 also includes phosphorylation of MPK3 and MPK6, which play a partially redundant role in inducing *FRK1* and *WRKY29* expression (Boudsocq et al., 2010). In *ilk1-1* seedlings, flg22 treatment induced maximum MPK3 and MPK6 phosphorylation by 6-min post-treatment (mpt) followed by a gradual decrease to 15 mpt (Fig. 4B); in wild type, MPK3 and MPK6 activation gradually increased over time to a maximum at 15 mpt (Fig. 4B). In line with this observation, *FRK1* and *WRKY29* induction was higher in *ilk1-1* and K222A-1 plants relative to the wild type, while ILK1-1 plants demonstrated similar or lower expression as the wild type (Fig. 4C).

These data suggest that the kinase activity of *ILK1* promotes PAMP responses and basal immunity in planta; we posit that *ILK1* modulates PAMP-triggered MAPK signaling, and operates downstream or independently of ROS production.

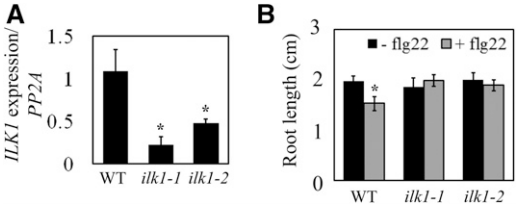

Figure 2. Mutants with reduced *ILK1* expression exhibit reduced root sensitivity to bacterial flg22. A, *ILK1* gene expression is reduced in *ilk1-1* and *ilk1-2* T-DNA insertion lines. Expression was quantified by qRT PCR in 4–6 biological replicates with two technical replicates and normalized to *protein phosphatase 2A* (*PP2A*) gene expression where * indicates significant difference from the wild type, $P < 0.05$. B, Flg22-induced root growth inhibition is absent in *ilk1-1* and *ilk1-2* seedlings. The seedlings were grown for 5 d prior to transfer to liquid MS media containing no flg22 or 100 nM flg22 and primary root length was quantified 10 d after transfer ($n = 10–16$) where * indicates significant difference in growth between the flg22-exposed and non-exposed plants within a line, $P < 0.05$.

Lack of *ILK1* Impairs NaCl and Mannitol Sensitivity

In addition to a role in immunity, previous studies associate *CML9* to high salt stress sensitivity (Magnan et al., 2008). To determine whether *ILK1* is similarly involved, the *ILK1* mutant lines were subjected to high NaCl or mannitol and germination was quantified. While *ilk1-1* seeds demonstrated salt insensitivity, germinating significantly more than the wild type, the ectopically expressing ILK1 lines demonstrated heightened sensitivity relative to the wild type (Fig. 5A). Similar trends were recorded when plates were supplemented with mannitol, indicating that *ILK1* expression is correlated with hyperosmotic stress sensitivity. Induction of the salt stress marker *Rd29A* (Yamaguchi-Shinozaki and Shinozaki, 1994) was also significantly lower in *ilk1-1* seedlings after exposure to high NaCl liquid media, while its expression in the ILK1-1 seedlings was at wild-type levels (Fig. 5B).

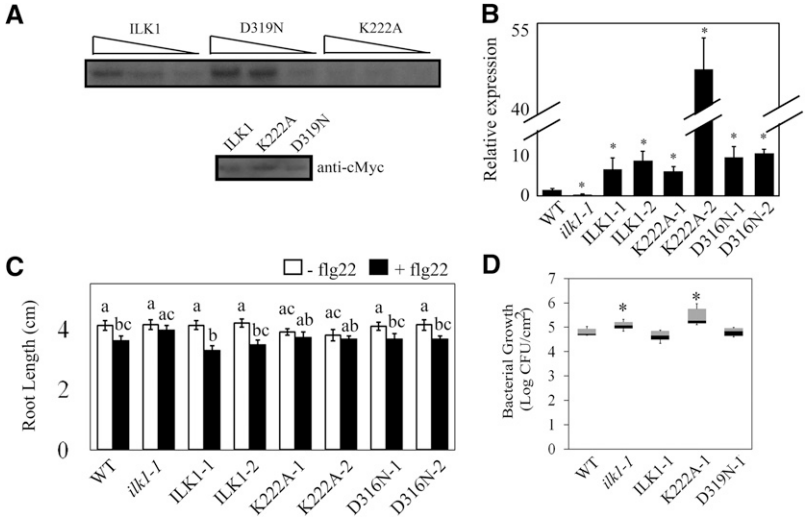

Figure 3. ILK1 activity is required for the flg22 response and bacterial resistance. A, Autophosphorylation activity of the cMyc-tagged ILK1, ILK1^{D319N}, or ILK1^{K222A} isoforms exposed to 5 mM Mn^{2+} and visualized by autoradiography. Equal loading of the protein was verified by western blot and decreasing relative concentrations (1, 0.5, and 0.25) of the enzymes were used as indicated by triangles. B, *ILK1* gene expression is enhanced in the *ilk1-1* lines transformed with clones containing *ILK1*, or the *ILK1*^{D319N} (increased kinase activity) or *ILK1*^{K222A} (decreased kinase activity) isoforms. Two lines for each construct were evaluated (i.e. ILK1-1, ILK1-2). Expression was quantified by qRT PCR in 4–6 biological replicates with two technical replicates and normalized to *PP2A* gene expression where * indicates significant difference from the wild type, $P < 0.05$. C, Flg22-induced root growth inhibition is regained in *ilk1-1* expressing *ILK1* or *ILK1*^{D319N} but not *ILK1*^{K222A}. The seedlings were grown for 5 d prior to transfer to liquid MS media containing no flg22 or 100 nM flg22 and primary root length was quantified 10 d after transfer ($n = 28$–32). The asterisk indicates a significant difference in growth between the flg22-exposed and non-exposed plants within a line, $P < 0.05$. D, Bacterial growth is enhanced in the *ilk1-1* knockdown and *ILK1*^{K222A}-expressing plants. The number of viable *P. syringae* pv. *tomato* Δ*hrcQ-U* bacteria in rosette leaves were counted 2 d after syringe inoculation ($n = 25$-36) where * indicates significant difference from the wild type, $P < 0.05$.

We examined next *ILK1* transcriptional regulation during stress. Previous work showed that *ILK1* expression was maintained constant in leaf and root tissues throughout development and in response to abiotic stress (Kilian et al., 2007; Chinchilla et al., 2008). Our measurements of *ILK1* transcript accumulation failed to detect significant changes in expression in wild-type seedlings treated with high NaCl, mannitol, or flg22 (Fig. 5C), confirming that transcriptional adjustment is not a significant regulatory means for *ILK1*.

Subcellular Localization of ILK1 Fusion Proteins in *Nicotiana benthamiana* and Arabidopsis

ILK1 is predicted to localize to the cytosol due to lack of any obvious localization signals (www.bar.utoronto.ca). To gain further insight into ILK1 subcellular localization, *ILK1*::*GFP* was expressed in *N. benthamiana* and the associated GFP signal was imaged using confocal microscopy. In leaf epidermal cells, the ILK1:GFP chimera colocalized with the HDEL endoplasmic reticulum (ER) retention sequence (Pearson correlation coefficient R = 0.70) and with the basic domain of CaM53 that localizes to the PM ($R = 0.84$; Fig. 6A; Gomord et al., 1997; Rodríguez-Concepción et al., 2000). The ILK1::GFP chimera also localized to the periphery of the cell under plasmolysis-inducing conditions where it was visualized in the Hechtian strands (Fig. 6B). In Arabidopsis seedlings expressing *ILK1*::*CFP* (ILK1-1 line), the CFP signal localized at the cell periphery in roots and shoots, as well as the proto-xylem (Fig. 6C). Taken together, our results suggest that ectopically expressed ILK1 associates with the inner side of the PM and ER membranes.

ILK1 Contributes to K^+ Accumulation during Stress, Which Is Required for flg22 Response

Potassium accumulation is reduced in plants under high NaCl conditions and is thought to be a major factor in determining tolerance to salt stress (Alemán et al., 2011). To determine if K^+ homeostasis is affected in *ilk1-1*, we measured the K^+ content in seedlings treated with high NaCl amounts or flg22. Interestingly, both *ilk1-1* and wild-type seedlings displayed a significant reduction of K^+ accumulation following NaCl or flg22 treatments (Fig. 7A). In contrast, ILK1-1 seedlings maintained control-level K^+ content under stress, accumulating significantly more K^+ than wild type (Fig. 7A). Loss of K^+ upon flg22 treatment has been documented at the cellular level (Jeworutzki et al., 2010), but a net K^+ loss at the seedling level has not been reported to date.

To test the significance of K^+ homeostasis in plant's response to flg22, we employed the root-growth

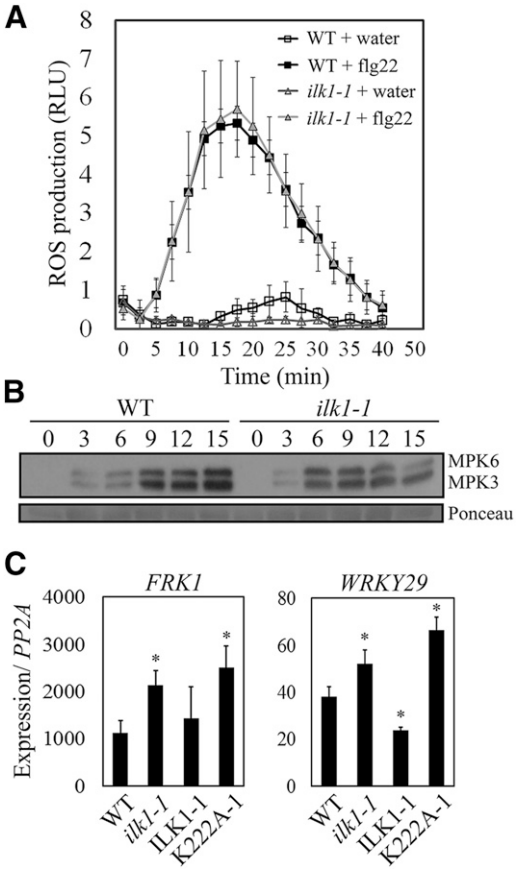

Figure 4. Some flg22-induced signaling responses are altered in *ilk1-1* plants. A, Flg22-induced ROS production is intact in *ilk1-1* plants. Leaf disks were exposed to 100 nM flg22 and ROS was quantified in relative light units immediately after exposure. Nine to 12 plants were measured in duplicate and the experiment was repeated three times. B, MAPK activation dynamics are altered in *ilk1-1*. Three to 5 seedlings were treated with 1 μM flg22 and harvested at the indicated time after exposure. MAPK phosphorylation was monitored by western blot with antip44/42 MAPK antibody. Ponceau staining is shown to assess equal loading. C, PAMP-triggered immunity-induced gene expression is enhanced in *ilk1-1* and *ILK1*^{K222A}-expressing seedlings. Two marker genes downstream of MAPK activation were evaluated for induction after treatment with 1 μM flg22 for 2 h compared to untreated seedlings. *FRK1* and *WRKY29* expression were quantified by qRT PCR in five biological replicates with two technical replicates and normalized to *PP2A* gene expression where * indicates significant difference from the wild type, $P < 0.05$.

inhibition assay to test wild-type responses in the presence of the K^+ channel blocker TEA (tetraethylammonium), thereby inhibiting K^+ fluxes while not affecting Ca^{2+} transport (Moran et al., 1988; Fu and Luan, 1998; Demidchik et al., 2010). While flg22 treatment resulted in root-growth inhibition in the absence of TEA, as expected, the presence of TEA at concentrations as low as 10 μM abolished this response in wild-type seedlings (Fig. 7B). The observed outcome was not due to a general repression of root growth, since TEA-treated plants produced root growth similar to the control.

Altogether, these results indicate that K^+ transport is altered in response to flg22 and that K^+ transport is required for flg22-induced root growth inhibition.

Ion Accumulation Changes After flg22 Treatment

Since K^+ accumulation appears to be important for flg22-induced responses, we evaluated whether K^+ transport is uniquely affected by flg22. To compare the effect of flg22 on other ions in the plant, the ionome of wild-type seedlings was examined between 15 and 180 min after flg22 treatment (Fig. 8A). Significant changes occurred as early as 15 min after flg22 treatment, including both transient increases/decreases (Mg^{2+}, P^{3-}, S^{2-}, and Zn^{2+}) and constant reductions (K^+,

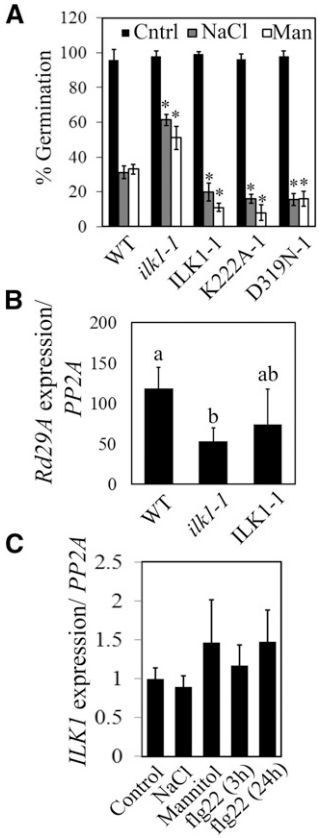

Figure 5. *ILK1* influences response to ionic or osmotic stress. A, Seed germination (radicle emergence) on plates containing 150 mM NaCl or 300 mM mannitol 3 d after vernalization. The average is expressed as a percentage of germination on control plates ($n = 100$) where * indicates significant difference from the wild type, $P < 0.05$. B, Salt-induced *Rd29A* expression is reduced in *ilk1-1* seedlings. Expression was normalized to *PP2A* expression and presented as the induction relative to the untreated control (set to 1) following application of 300 mM NaCl for 8 h ($n = 4$ biological replicates) where * indicates significant difference from the wild type, $P < 0.05$. C, Stress does not alter the expression of *ILK1*. Wild-type seedlings were subjected to control conditions or 300 mM NaCl for 5 h, 400 mM mannitol for 5 h or 1 μM flg22 for 3 or 24 h and expression was calculated as described in (B) ($n = 3$).

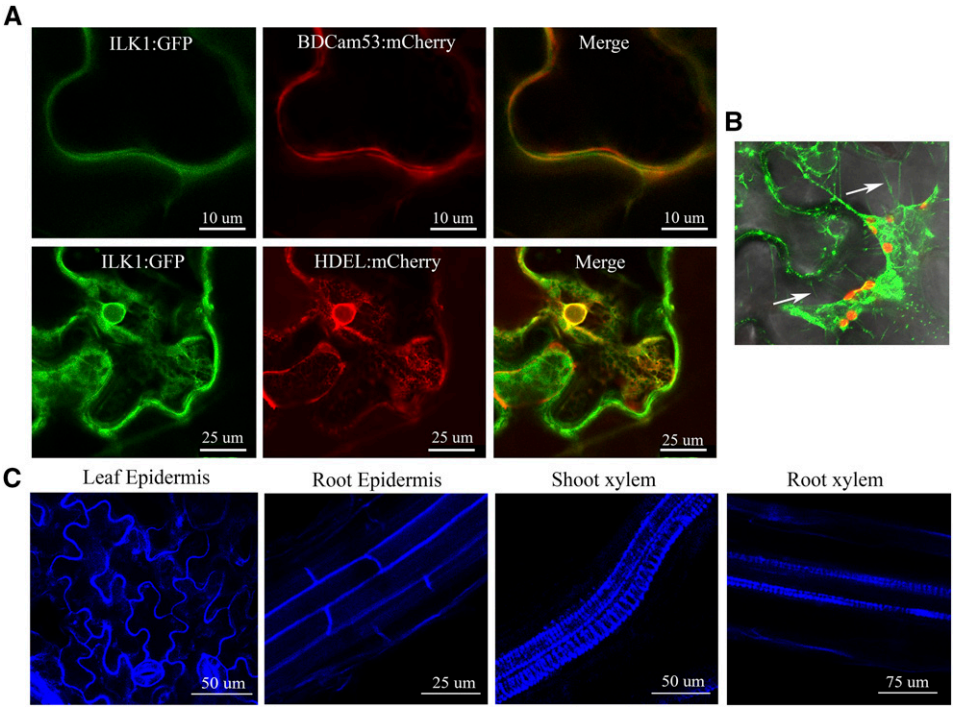

Figure 6. ILK1 fusion proteins localize to the cell periphery. A, Transiently expressed ILK1-GFP colocalizes with the endoplasmic reticulum HDEL:mCherry marker and the plasma membrane BDCam53:mCherry marker in *N. benthamiana* leaf epidermis cells ($n = 5$). B, ILK1-GFP localizes to Hechtian strands (indicated by white arrows) in plasmolized *N. benthamiana* leaf epidermis cells following treatment with 1 M NaCl ($n = 4$). C, Stably expressed ILK1-CFP localizes to the proto-xylem and the periphery of leaf and root cells in Arabidopsis 3-week-old seedlings ($n = 5–10$).

Na^{2+}, and Mn^{2+}) in ion content over 3 h. To determine if *ILK1* influences ion content in the absence of stress, we compared the ionomes of wild type, *ilk1-1*, and ILK1-1 seedlings and found no significant differences between wild type and the two mutant lines (Fig. 8B). Next, the ion content was compared between lines following flg22 application. Unlike wild type and *ilk1-1*, which showed a net loss of K^+ following flg22 application, the ILK1-1 line maintained constant tissue K^+ concentrations over time, consistent with the trends in Figure 7A. In addition, the *ilk1-1*, but not ILK1-1, seedlings exhibited higher Mn^{2+} content throughout the time course; Ca^{2+} decreased over time in *ilk1-1* while it increased in the ILK1-1 line (Fig. 8C; Supplemental Data S1).

Taken together, our results indicate that flg22 has a significant effect on ion homeostasis in intact Arabidopsis seedlings and that *ILK1* impacts K^+, Mn^{2+}, Mg^{2+}, S, and Ca^{2+} homeostasis following PAMP perception.

ILK1 Interacts with the HAK5 Potassium Uptake Transporter and Is Required for Growth in Limiting K^+ Conditions

We hypothesized that *ILK1* may be interacting with and regulating a cellular component involved in osmoregulation or ion homeostasis during stress. To identify potential ILK1 interactors, we took an unbiased proteomics approach using two methods. First, functional protein microarrays containing 15,000 proteins were probed with purified ILK1-V5 and anti-V5 Cy3-labeled antibody, allowing identification of in vitro protein-ILK1 complexes (Brauer et al., 2014). Second, in vitro phosphorylation targets ILK1 were identified using in a kinase client assay (KiC) where purified ILK1-cMyc was incubated with a peptide library and phosphorylation of peptides was quantified by mass spectrometry (Ahsan et al., 2013). These approaches revealed a number of putative ILK1 interactors including several transporters (Supplemental Table S3). Among the interactors were two transporters from the K^+ uptake permease family (KUP)—KUP5 and the high affinity K^+ transporter HAK5. While little is known about the function of *KUP5* in plants, *HAK5* is important for growth maintenance in K^+-limiting environments and during salt stress (Nieves-Cordones et al., 2010; Rubio et al., 2010). Since the KiC assay indicated that ILK1 phosphorylates a peptide derived from the N-terminal cytosolic domain of HAK5, we hypothesized that HAK5 is a functional interaction partner of ILK1.

We tested ILK1-HAK5 interaction in Arabidopsis protoplasts by SLCA using full-length ILK1 and the N- or C-terminal cytosolic portions of HAK5. High levels of luciferase signal indicated that ILK1 interacted with both fragments of HAK5, while CML9 did not (Fig. 9A). To confirm this interaction in the absence of other plant proteins, protein interactions were validated in *Xenopus* oocytes using the bimolecular fluorescence complementation assay. Full-length HAK5, ILK1, and CML9 were each fused to the complementary halves of the YFP, and the cRNAs were coinjected into oocytes and analyzed by confocal microscopy. Coinjection of cRNA encoding *ILK1* with *HAK5* resulted in a significant YFP signal, indicating a direct interaction of these protein products (Fig. 9B, top left image). In contrast, no fluorescence was observed in cells coinjected with *HAK5*

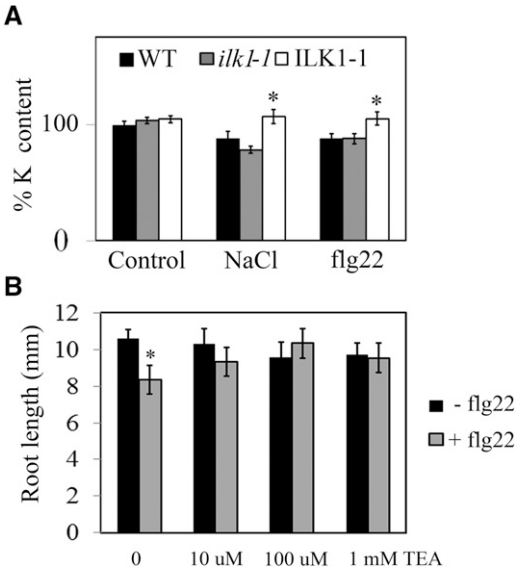

Figure 7. Changes in K^+ homeostasis during stress are necessary for flg22-induced root growth response. A, K^+ content is reduced during stress. Comparison of K^+ content in NaCl (300 mM, 8 h) and flg22-treated (1 μM, 15 min) seedlings relative to untreated seedlings (set at 100%, $n = 4–20$) where * indicates significant difference from the wild type for a given treatment, $P < 0.05$. B, Flg22-induced root growth inhibition can be rescued by the K^+ channel blocker TEA. The seedlings were grown for 5 d prior to transfer to modified liquid MS media with 2 mM K^+ (instead of 20 mM in unmodified MS media) containing no flg22 or 100 nM flg22 supplemented with the indicated concentration of TEA. Primary root length was quantified 10 d after transfer ($n = 10–16$) where * indicates significant difference from the nonflg22 treatment, $P < 0.05$.

and *CML9* cRNA (Fig. 9B, top- and bottom-right images), regardless of the presence or absence of unlabeled *ILK1* cRNA. Together with the data presented in Figure 1, this suggests that ILK1-HAK5 and ILK1-CML9 interactions occur in vivo, while CML9 and HAK5 do not interact.

To determine if HAK5 is a phosphorylation target of ILK1, we performed a radioactive kinase assay with the N-terminal cytosolic domain of HAK5; however, phosphorylation was not detected under the tested conditions (data not shown). Next, we explored the possibility that ILK1 modulates HAK5 by acting at a step in HAK5 synthesis, as previously shown for other K^+ transporters (Held et al., 2011). Transient co-expression of *HAK5*, *ILK1*, and *CML9* in *N. benthamiana* leaves resulted in HAK5 protein accumulation in the membrane fraction of leaf extracts, while HAK5 could not be detected when expressed alone or in combination with either ILK1 or CML9 (Fig. 9C).

Physiological studies have shown that *HAK5* is required for growth under limiting K^+ conditions (Rodríguez-Navarro and Rubio, 2006; Qi et al., 2008). To determine if *ILK1* is similarly involved in response to limiting K^+ conditions, *ilk1-1* plants were grown alongside the previously characterized *hak5-3* knockout mutant in media that contained 10 μM K^+. Relative to wild-type plants, the *hak5-3* seedlings struggled to maintain growth under these conditions (Fig. 9D). The *ilk1-1* and K222A-1 seedlings were also stunted relative to wild type under the low K^+ conditions, while ILK1-1 and D319N-1 lines supported wild-type-level growth. No changes in *HAK5* expression were observed in *ilk1-1*

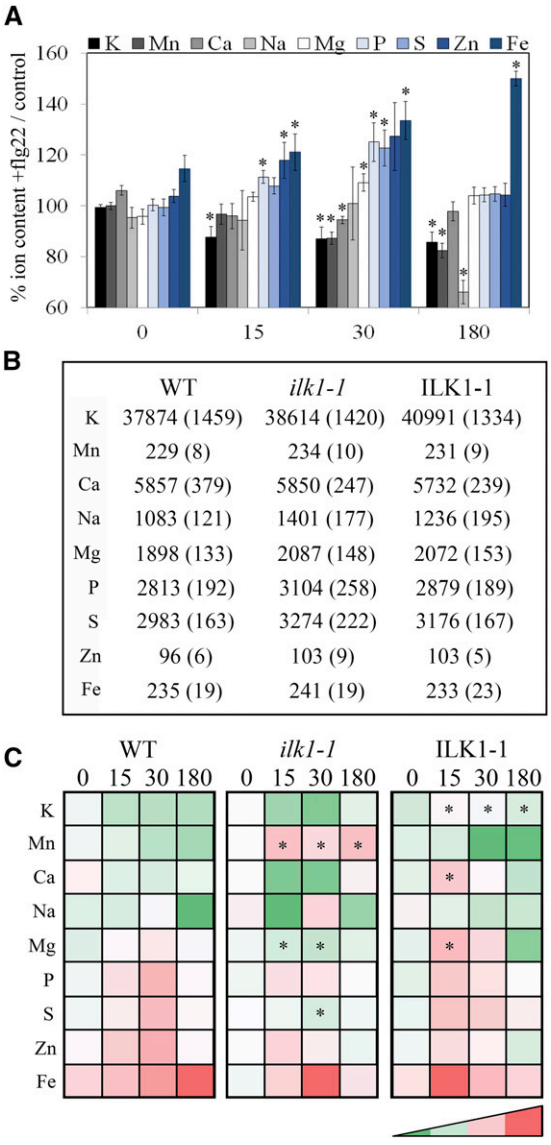

	WT	*ilk1-1*	ILK1-1
K	37874 (1459)	38614 (1420)	40991 (1334)
Mn	229 (8)	234 (10)	231 (9)
Ca	5857 (379)	5850 (247)	5732 (239)
Na	1083 (121)	1401 (177)	1236 (195)
Mg	1898 (133)	2087 (148)	2072 (153)
P	2813 (192)	3104 (258)	2879 (189)
S	2983 (163)	3274 (222)	3176 (167)
Zn	96 (6)	103 (9)	103 (5)
Fe	235 (19)	241 (19)	233 (23)

Figure 8. Ion homeostasis changes during flg22 Induction. A, Ionomic profile of wild-type seedlings treated with 1 μM flg22 normalized to the untreated control 15, 30, and 180 min after treatment ($n = 4$), where * indicates significant difference from the wild type for a given time point, $P < 0.05$. B, Wild type, *ilk1-1*, and ILK1-1 have identical ionomic profiles under control conditions. Means in mg/g dry weight for 15 replicates are presented alongside SE in parentheses. C, The *ilk1-1* and ILK1-1 show different ionomic responses to flg22 relative to wild type. The heat map indicating the relative ion content of two-week old seedlings treated with 1 μM flg22. Each ion is normalized to the untreated control where red indicates higher content while green indicates lower content ($n = 4$), where * indicates significant difference from the wild type at the given time, $P < 0.05$.

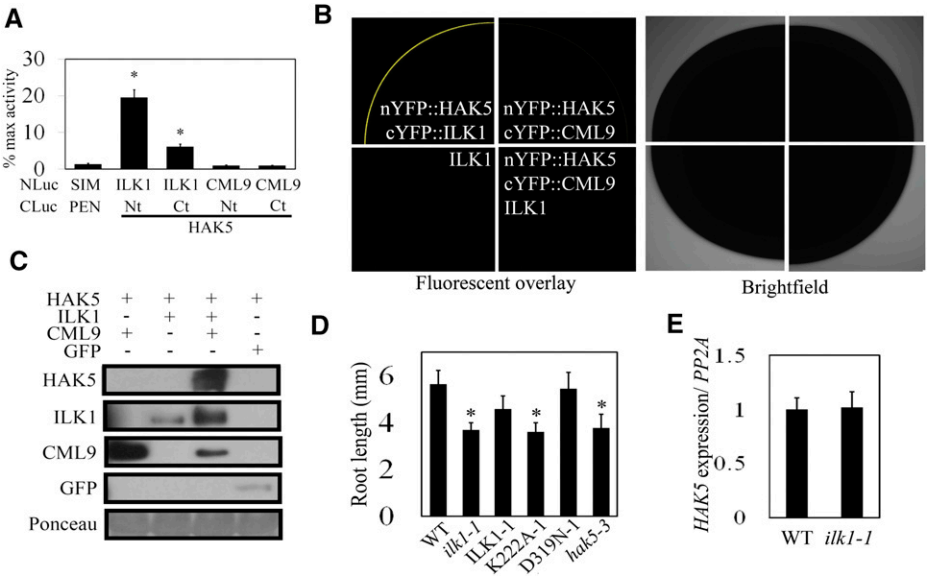

Figure 9. ILK1 interacts with the HAK5 K^+ uptake transporter and promotes growth in low K^+ conditions. A, ILK1 and HAK5 cytosolic domains interact in Arabidopsis protoplasts. Luciferase signal resulting from interaction between bait (NLuc) and prey (CLuc) fusion proteins is normalized to the signal produced by a positive control pair (NLuc-H2A, CLuc-H2B). Four replicates from three independent experiments for each pair were used where * indicates significant difference from the negative control (NLuc-SIM, CLuc-PAN, $P < 0.05$). B, Images showing interaction of ILK1 with full-length HAK5 by bimolecular fluorescence complementation in *Xenopus* oocytes. The image shows the fluorescence (left panel) and bright field (right panel) confocal microscopy images of one-quarter of oocyte cells expressing the constructs indicated in each set. No interaction between nYFP::HAK5 and cYFP::CML9 was observed even upon coinjection with the untagged ILK1. Untagged ILK1 was transformed into cells as a negative control for background autofluorescence ($n = 6$). C, HAK5 accumulates when co-expressed with ILK1 and CML9. HAK5-GFP protein accumulation in the membrane fraction of *N. benthamiana* leaves was evaluated by western blot. HAK5 was co-expressed with GFP, CML-cMyc, or ILK1-cMyc, which are visible in the soluble fraction. Equal loading of total protein extract was verified by Ponceau stain. D, Primary root length under limiting K^+ conditions (10 μM) 6 d after germination where * indicates significant difference from the wild type, $P < 0.05$. E, *HAK5* expression is unaffected in *ilk1-1* plants. The mean *HAK5* expression from six replicates is presented, where expression is normalized to *PP2A*.

seedlings, indicating that the stunted *ilk1-1* growth is not due to an effect of *ILK1* on *HAK5* expression (Fig. 9E).

These results suggest that *ILK1* promotes HAK5 accumulation in conjunction with *CML9*; furthermore, they suggest that *ILK1* modulates high-affinity K^+ transport or plant response to K^+ deficiency in a kinase-dependent manner.

Lack of ILK1 and HAK5 Impairs flg22-Induced Signaling and Cellular Ion Fluxes

Given that ILK1 interacts with HAK5 and K^+ accumulation is important for the flg22 response, we reasoned that HAK5 might be required for flg22 sensitivity. To test this hypothesis, we exposed the *hak5-3* mutant to flg22 and quantified root-growth inhibition. While the *hak5-3* exhibited wild-type growth under control conditions, it failed to show inhibition of the root-growth postflg22-treatment (Fig. 10A). Similarly to the *ilk1-1* mutant (i.e. Fig. 4C), *hak5-3* also had a significantly higher induction of *FRK1* and *WRKY29* expression in response to flg22 (Fig. 10B).

During stress, anion efflux across the cell's PM results in a depolarization of the membrane potential and induction of K^+ efflux, presumably to charge-balance anion efflux. To test if *HAK5* and *ILK1* play a role in flg22-induced PM depolarization, leaf mesophyll PM membrane potential was monitored using microelectrodes impaled into leaf cells. Consistent with previous reports (Jeworutzki et al., 2010), addition of flg22 to the extracellular media resulted in PM depolarization after a 2-min delay, reaching a steady depolarized state within 3 min (Fig. 10C). The time-course change in membrane potential in both the ILK1-1 and K222A-1 leaf cells resembled that recorded in wild type (Fig. 10C). In contrast, the *ilk1-1* and *hak5-3* cells demonstrated a significantly slower depolarization rate, taking approximately 5 min longer to reach a similar steady depolarized state (Fig. 10, D and E). This indicates that *HAK5* and *ILK1* contribute to flg22-induced ion fluxes at the PM and that ILK1's role in this process is independent of its kinase activity.

To determine if K^+ transport is contributing to the PM depolarization, we pretreated wild-type leaves with the K^+ channel blocker TEA and exposed them to flg22. TEA-treated leaf disks displayed a delayed PM

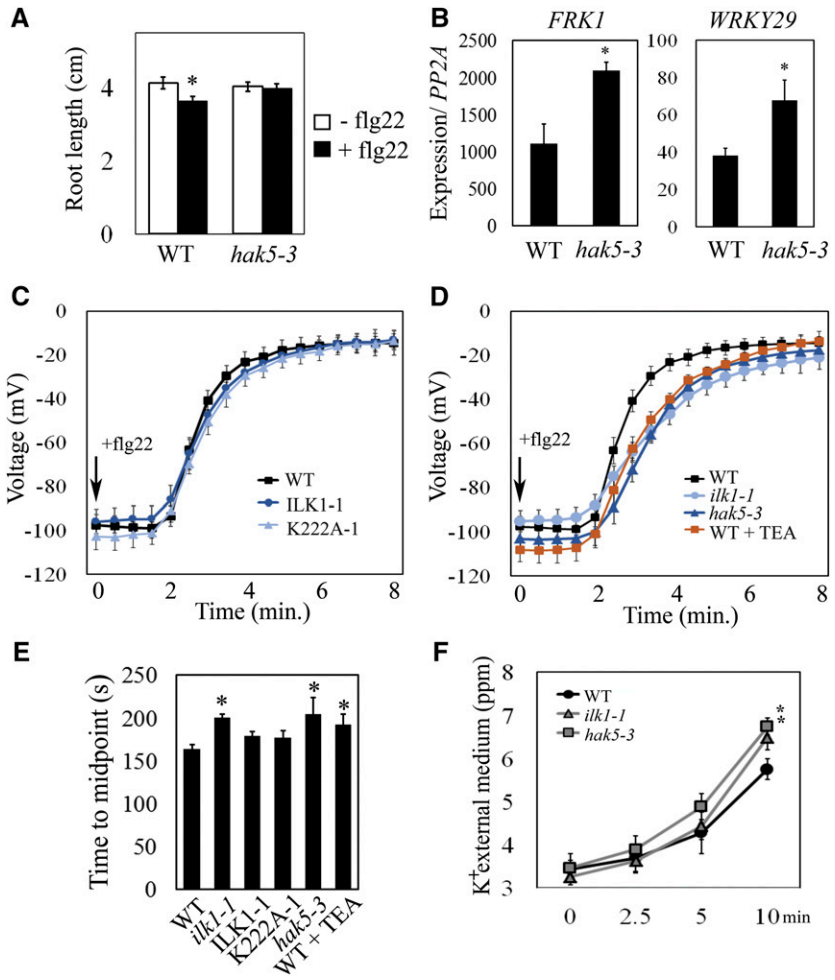

Figure 10. Loss of *HAK5* and *ILK1* Alters flg22 signaling responses. A, Flg22-induced root-growth inhibition is disrupted in *hak5-3* mutants. Seedlings were grown for 5 d prior to transfer to liquid MS media containing 100 nM flg22 and primary root length was quantified 10 d after transfer (n = 24–32), where * indicates significant difference from the nonflg22 treatment within a line, $P < 0.05$. B, Flg22-induced marker gene induction is disrupted in *hak5-3* mutants. *FRK1* and *WRKY29* expression were quantified after treatment with 1 μM flg22 for 2 h. Expression from five replicates was normalized to *PP2A* and expressed relative to untreated seedlings where * indicates significant difference from the wild type, $P < 0.05$. C and D, Membrane depolarization following 10 nM flg22 application in leaf mesophyll cells of the wild type (n = 12), ILK1-1 and K222A-1 plants (n = 5–7), *ilk1-1* and *hak5-3* plants (n = 9–12) and wild-type plants pretreated with 10 mM TEA for 1 h (n = 8). E, Midpoint of the flg22-induced depolarization time course between the onset and the final steady state for each genotype tested in (C) and (D), where * indicates significant difference from the wild type, $P < 0.05$. F, K^+ concentration of the extracellular media surrounding flg22-treated leaf disks from (C) and (D), where * indicates significant difference from the wild type for a given time point, $P < 0.05$.

depolarization, similar in scale to the *ilk1-1* and *hak5-3* mutants (Fig. 10, D and E). Furthermore, flg22-treated *ilk1-1* and *hak5-3* leaf disks accumulated higher K^+ in the surrounding media relative to the wild type (Fig. 10F).

Together, these observations suggest that *HAK5* and *ILK1* contribute to flg22-induced responses including both early changes in cellular ion homeostasis as well as longer-term responses such as growth suppression.

DISCUSSION

Here, we describe two, to our knowledge, novel components of the flg22 response pathway, ILK1 and its interacting partner, the HAK5 K^+ transporter. Our data supports a preliminary model where ILK1 and HAK5 are part of an flg22-induced signaling pathway where ILK1 functions as a kinase to promote growth inhibition downstream or independent of ROS production, and modulate MPK3 and MPK6 signaling (Fig. 11A). This pathway may involve K^+ transport since abolishment of K^+ transport recapitulated *ilk1-1* and *hak5-3* immune phenotypes and both *HAK5* expression and ILK1 kinase activity are involved in the response to K^+ limitation. ILK1-dependent signaling is functionally relevant for basal immunity since ILK1 activity is necessary to limit intracellular proliferation of a weakened *P. syringae* pv. *tomato* strain (Fig. 3D). Our findings provide, to our knowledge, the first evidence that K^+ transport is important for the generation of PAMP responses in plants, and place *ILK1* and *HAK5* as potential mediators of K^+-dependent signals.

Recognition of PAMPs and host-derived damage-associated molecular patterns triggers a large K^+ efflux from both plant and animal cells (Perregaux and Gabel, 1994; Walev et al., 1995; Colomar et al., 2003; Mithöfer et al., 2005). Several groups have reported that this K^+ efflux, or rather a low intracellular K^+ concentration, functions as a signal to induce downstream immune responses (Seydel et al., 2001; Scheel et al., 2006; Pétrilli et al., 2007; Arlehamn et al., 2010). For example, in animal cells the toll-like receptor TLR4 binds the bacterial PAMP LPS (lipopolysaccharide) and induces K^+ efflux through the MaxiK K^+ channel, activating signal cascades and release of the pro-inflammatory tumor necrosis factor-α (Scheel et al., 2006). Blocking K^+ efflux using specific MaxiK blocking agents or with TEA abolished LPS-induced tumor

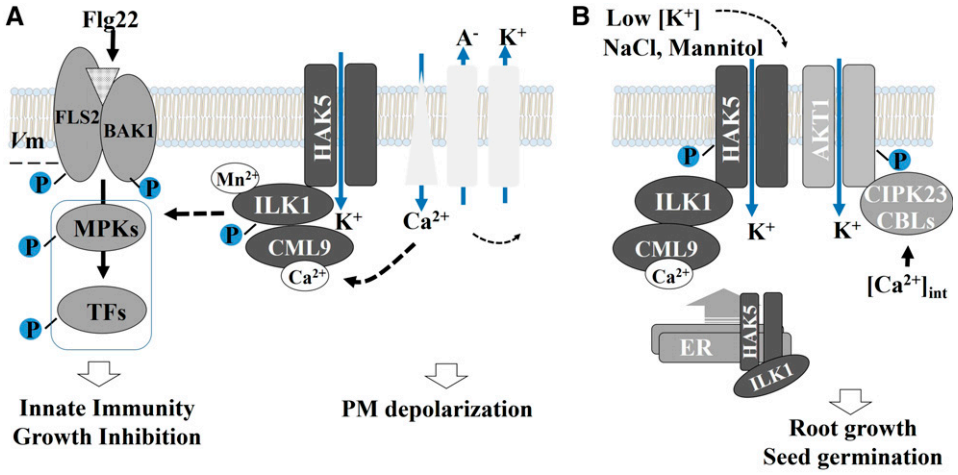

Figure 11. Preliminary model of ILK1's roles during stress. A, A model of possible signaling-related functions of *ILK1* in PAMP-triggered innate immunity. After flg22 recognition by BAK1-FLS2, Ca^{2+} influxes trigger anion export, which depolarizes the membrane and induces K^+ efflux. Calcium sensors such as CML9 may modulate ILK1 kinase activity that phosphorylates HAK5 or other signaling molecules to activate an unknown signaling pathway. This pathway, which may involve K^+-sensing to repress early MPK3/MPK6 signaling, has a net positive effect on plant innate immunity and regulates growth in response to PAMPs. Flg22-triggered membrane depolarization involves rapid activation of several unknown channels, which may include GLR3.3 and are influenced by HAK5 and ILK1 in a kinase-independent manner. B, A model of proposed *ILK1* roles in potassium transport for plant responses to abiotic stress. During osmotic stress and limited K^+ supply, ILK1 and CML9 promote HAK5 maturation and transport to the membrane. Low intracellular K^+ concentrations lead to accumulation of intracellular Ca^{2+} and signaling through CML9/ILK1 or CBLs/CIPK23, which activate HAK5.

necrosis factor-α formation, indicating that intracellular K^+ status stimulates PAMP signaling. It is not currently known how the K^+ status is detected by the cell, although conformational changes of signaling molecules have been proposed (Pétrilli et al., 2007). In support of this idea, a recent study demonstrated that K^+ efflux was required to induce complex formation between an intracellular PAMP receptor (NLRP3) and a kinase (NEK7) to activate signaling (He et al., 2016). Interestingly, ILK has recently been shown to function as a kinase in activating TNF-α production downstream of TLR4-mediated recognition of LPS, although it is not known if this is K^+-efflux dependent (Ahmed et al., 2014).

In plants, K^+ status may be detected by K^+ transport systems including HAK5 and AKT1 as well as by other enzymes such as the pyruvate kinase, which is activated by increased cytosolic K^+ concentrations (Wang and Wu, 2010). HAK5 and AKT1 K^+ uptake activity are both induced by K^+ limitation, likely through changes in phosphorylation status. For example, high-affinity K^+ uptake through the AKT1 channel is regulated by Ca^{2+}-responsive calcineurin B-like proteins 1–9 (CBL), which recruit CIPK23 to the PM where it phosphorylates AKT1 (Lee et al., 2007). Our data indicate that ILK1 phosphorylates the N-terminal of HAK5 in vitro (Supplemental Table S3), and that ILK1 activity contributes to growth during extreme K^+-limitation (Fig. 9D), where HAK5 is the only transport system contributing to K^+ uptake (Rubio and Rodríguez-Navarro, 2000). Although HAK5 phosphorylation has not yet been shown in planta, several studies strongly indicate that HAK5 activity status is modulated by phosphorylation of its N terminus (Jones et al., 2009; Rubio et al., 2014; Ragel et al., 2015; Scherzer et al., 2015). Co-expression of the CBLs and CIPK23 also increases HAK5 transport through CIPK23 activity, indicating that HAK5 conformation may be regulated by phosphorylation during K^+ deficiency (Ragel et al., 2015; Scherzer et al., 2015). However, HAK5 regulation may require additional uncharacterized components.

We showed that ILK1 interacts with a Ca^{2+}-sensing protein CML9, and postulate that the CML9-ILK1 module may influence HAK5 function during flg22 signaling in response to Ca^{2+} influx. Although CML9 inhibited ILK1 activity regardless of the presence or absence of Ca^{2+} (Fig. 1E), the conditions in our assays may not have been within the sensitivity range of CML9 since CML9 is a divergent member of the CaM family that may have a lower sensitivity to Ca^{2+} than other CMLs (Zielinski, 2002). ILK1 may function in parallel or in coordination with the CBL/CIPK pathway to modify K^+ transport, thereby activating K^+-sensing proteins and signal transduction. Alternatively, changes in HAK5 conformation during K^+ limitation may trigger ILK1 autophosphorylation, and ILK1-dependent phosphorylation of signaling proteins. A potential component of the ILK1 pathway could include the 14-3-3 Ω protein, which consistently co-purifies with ILK1 (Supplemental Fig. S2). In Arabidopsis, 14-3-3 Ω protein has been shown to interact with BZR1, a transcription factor involved in brassinosteroid signaling

and thought to have an important role in mediating growth suppression during immunity (Gampala et al., 2007; Lozano-Durán and Zipfel, 2015). A functional study of ILK1-interacting proteins should provide more insight into the identity of other contributors of the ILK1-dependent signaling pathway during immunity.

In addition to a kinase-dependent role in immunity, our results suggest that ILK1 has a kinase-independent role to promote HAK5 accumulation, together with CML9 (Figs. 9, B and C; 11B). Many PM-localized transporters and receptors traffic out of the ER and travel to the PM alongside escort proteins to improve stability and structural conformation (Lee et al., 2011; Kolb et al., 2014). In conditions of K^+ deficiency, HAK5 accumulation shifts from the ER to the PM (Qi et al., 2008), suggesting that its secretion is another way by which HAK5 activity is regulated. The regulation of HAK5 trafficking may be significant for longer-term responses to K^+ deficiency, including seed germination, but is less likely to explain ILK1's kinase-independent role in rapid responses, including flg22-induced PM depolarization (Fig. 10D). In our study, PAMP treatment induced K^+ loss in seedlings and leaf mesophyll cells (Figs. 8A and 10F) and ILK1 and HAK5 expression attenuated the cellular K^+ loss (Fig. 10F). The timing of K^+ loss in mesophyll cells corresponded with PM depolarization, and seemed to contribute to the rate of depolarization since TEA treatment slightly delayed this process (Fig. 10D). K^+ is critical for the maintenance of membrane polarization; a high external K^+ promotes membrane depolarization (Spalding et al., 1999). However, the amplitude of depolarization under these high K^+ conditions is lower than PM depolarization upon PAMP stress, indicating that different mechanisms are at work. Jeworutzki et al. (2010) showed that PAMP-triggered PM depolarization is initiated by an increase in cytosolic Ca^{2+} that activates anion efflux, followed by activation of K^+ efflux channels. ILK1's kinase-independent role in promoting rapid flg22-induced PM depolarization may be due to the interaction between transport systems. For example, HAK5 transport could be influencing other channels at the PM such as the Glu receptor-like channel *GLR3.3*, which promotes Ca^{2+} influx during immunity (Qi et al., 2006; Li et al., 2013).

Plant and animal ILKs share several characteristics, including ankyrin repeats, a degenerate kinase domain, an unusual Mn^{2+}-dependent activity, and the ability to phosphorylate tubulin (Fig. 1; Chinchilla et al., 2008; Maydan et al., 2010). In animals, ILKs initiate signal transduction through both kinase-dependent and -independent mechanisms to mediate cell proliferation, growth, and immune responses (Hannigan et al., 2011). We describe a plant *ILK* with a kinase-dependent function in plant immunity and a kinase-independent function in maintaining K^+ transporter accumulation and ion fluxes during stress. ILKs emerge as multivalent proteins able to mobilize distinct partners to modulate signaling across kingdoms.

MATERIALS AND METHODS

Plant Material, Growth Conditions, and Stress Treatments

Columbia ecotype Arabidopsis plants were propagated as described previously in Lee et (al., 2011). Expression analysis, ion content, and MAPK induction experiments were performed on 2-week-old seedlings grown in liquid Murashige and Skoog (MS) media containing 3% Suc. Germination assays were performed on 10-cm-diameter petri dishes containing 25 mL of 1/2 MS media with 0.7% Phytoagar and sterile mannitol or NaCl at the indicated concentrations. Flg22-induced root growth inhibition was measured as indicated after 10 d of growth on solid MS media with 0.7% Phytoagar. Unless otherwise indicated, all experiments were conducted three times and significance ($P \leq 0.05$) is indicated by an asterisk, as calculated using a *t*-test. To generate *ilk1-1*, a segregating T-DNA insertion line was obtained from The Arabidopsis Information Resource (SAIL-760-C05, AT2G43850). Homozygous T3 *ilk1-1* insert and azygous lines were selected by PCR after back-crossing to Columbia plants and one round of selfing. The homozygous *ilk1-2* line was obtained from The Arabidopsis Information Resource (WiscDsLoxHs009_11D).

Split Luciferase Complementation Assays

The C-termini of proteins of interest were fused to either the N-terminal or C-terminal of *Renilla reniformis* luciferase and were coexpressed in Arabidopsis protoplasts. The cloning, protoplast preparation, and split-luciferase complementation assays were performed as described, using a Veritas microplate luminometer (Turner BioSystems, Sunnyvale, CA; Fujikawa and Kato, 2007). Expression vectors expressing a negative control protein pair, *NLuc-SIM* and *CLuc-PAN*, were constructed by inserting coding DNA sequences of SIAMES (AT5G04470) and PERIANTHIA (AT1G68640) in pDuExAn6 and pDuExDn6 (Kato and Jones, 2010), respectively.

Bimolecular Fluorescence Complementation Assays

The cDNA of HAK5, ILK1, and CAM9 were cloned into oocyte (bimolecular fluorescence complementation) expression vectors by an advanced uracil excision-based cloning technique described previously in Nour-Eldin et al. (2006). Heterologous expression in *Xenopus* oocytes and YFP visualization (2–6 d after injection) were performed as described in Ligaba et al. (2013).

Constructs and Arabidopsis Transformation

The *ILK1* cDNA clone was obtained from ABRC and subcloned into the pDONRzeo Gateway. Following confirmation by sequencing, point mutations were made in the sequence using PCR and all constructs were cloned into pEARLEYGATE103 for localization ($P_{CaMV35S}$:*ILK1-GFP*), pEARLEYGATE102 for complementation ($P_{CaMV35S}$:*ILK1-CFP*), pYL436 for protein purification, pDuEx-Bait/pDuEx-Prey for split-luciferase complementation assay, and pNB1YNu/pNB1YCu for bimolecular fluorescence complementation (Nour-Eldin et al., 2006; Fujikawa and Kato, 2007). T1 seeds of *ILK1-CFP*, *K222A-CFP*, and *D319N-CFP* lines were selected by PCR for the CFP gene and expression of *ILK1* was confirmed by qRT PCR.

Kinase Activity Assays

Recombinant C-terminal TAP-tagged proteins were purified from *N. benthamiana* leaves by immunoprecipitation as described in detail previously in Brauer et al. (2014). Total protein content was quantified by Bradford assay and the presence of the V5 or cMyc-tagged protein was visualized by western blot. To measure kinase activity, 650–700 ng of the protein preparation was incubated with kinase buffer to a final volume of 20 μL (5 mM Tris-HCl pH 7.5, 0.25 mM DTT, 1.25 μM $^{\gamma}P^{32}$-ATP, and 0.1 mg/mL substrate), and the amount of co-factor indicated in the figure legend. To verify consistent loading, a duplicate reaction was separated on a SDS-PAGE gel, transferred to a membrane, and exposed to Ponceau staining.

Bacterial Infection Assays

The bacterial strains were grown overnight at 30°C prior to being suspended in infiltration medium (10 mM $MgCl_2$) to 3×10^5 CFU/mL and infiltrated into 4–6-week-old plants using needleless syringes. The plants were grown in high

humidity for 2 d and tissue was harvested and quantified as described in Singh et al. (2014).

Oxidative Burst Assay

Duplicate 6-mm leaf disks were collected from 9 to 12 plants per line and placed adaxial side up in deionized water overnight in a 96-well plate. The following day, the water was replaced with 100 μL of detection buffer (17 μL/mL luminol (Sigma-Aldrich, St. Louis, MO), 20 μL/mL horseradish peroxidase (Sigma-Aldrich) containing 100 nM flg22. The plate was measured for luminescence for 45 min after buffer application in a Synergy 2 microplate reader (BioTek Instruments, Winooski, VT). The relative light units were calculated for each time point within an experiment.

MAPK Phosphorylation Assay

Protein was extracted from three 2-week-old seedlings following exposure to flg22 in 0.1 mM $MnCl_2$ as described in Brauer et al. (2014) and quantified using the Bradford assay. Equal amounts of total protein was separated and probed with antip42/44 MAPK antibodies (1:1000; Cell Signaling Technology, Danvers, MA), anti-rabbit-HRP antibodies (1:2000; Sigma-Aldrich) and were stained with Ponceau after exposure.

RNA Extraction and qRT PCR

RNA isolation and cDNA synthesis for expression analysis of 2-week-old seedlings with and without stress treatments were performed as described previously in Moreau et al. (2013). Biological replicates contained 15–20 seedlings and qRT PCR was performed in 20 μL reactions using iTAQ SYBR Green (BioRad, Hercules, CA).

Subcellular Localization of ILK1

Nicotiana benthamiana leaves were co-transformed with the $P_{CaMV35S}$: *ILK1-GFP* and $P_{CaMV35S}$:*HDEL-mCherry* or $P_{CaMV35S}$:*BDCaM53-mCherry* constructs according to Popescu et al. (2007). Red, cyan, and green fluorescence was confirmed using a lambda scan and imaged with a confocal laser scanning microscope using a 40× dry objective or 63× water immersion objective (SP5; Leica Microsystems, Wetzlar, Germany). Images were processed with the Leica LAS-AF 1.8.2 software (Leica Microsystems). Colocalization of the GFP signal with mCherry signal was confirmed using the software Image-Pro (v. 6.3; Media Cybernetics, http://www.mediacy.com/). For localization in Arabidopsis, stably transformed lines ILK1-1 expressing $P_{CaMV35S}$:*ILK1-CFP* were imaged using the same method.

Ion Content Measurement

Replicate samples containing 25 2-week-old seedlings were exposed to the indicated treatment before rinsing and drying at 50°C. The dried tissue was homogenized and analyzed by inductively coupled plasma emission spectrometry as previously described in Maron et al. (2008).

Electrophysiology

To determine membrane depolarization in leaf mesophyll cells from 5 to 10-week-old rosette leaves, the epidermis was removed from the underside of the leaf and the leaf was affixed to 5-mm-diameter circular glass slides using double-sided adhesive tape. The samples were incubated in a bath solution of 0.1 mM KCl, 1 mM $CaCl_2$, and 1 mM MES/bis-Tris propane pH 6.0 for 4 h prior to measuring flg22-induced membrane depolarization using the method described in Jeworutzki et al. (2010).

Mass Spectrometry Analysis and Kinase Client Assay

Autophosphorylation of purified recombinant kinases (ILK1 and its D319N mutant) was detected using a LTQ Orbitrap XL ETD mass spectrometer (Thermo Fisher, San Jose, CA). The kinase assay was conducted in kinase buffer (20 mM HEPES-KOH pH 7.4, 5 mM $MgCl_2$ or $MnCl_2$, 1 mM DTT, 2 mM ATP; Ahsan et al., 2013). The kinase client assay was performed with 5 mM $MnCl_2$ with purified ILK1 and a mixture of approximately 210 synthetic peptides (8 μM) per sample from a library of 2095 peptides that were designed based on the in vivo phosphoproteomic dataset available on the P^3DB Web site (http://www.p3db.org/). For mining kinase client assay results, raw MS files were searched against a decoy database consisting of the random complement of the sequences comprising the peptide library, using SEQUEST (Proteome Discoverer, v. 1.0.3; Thermo Fisher). Identification data were evaluated using the XCorr function of SEQUEST, and phosphorylation-site localization was performed using phosphoRS (Proteome Discoverer; v. 1.0.3; Thermo Fisher). The XCorr values for each charge state were set to default, and no decoy hits were allowed. Peptide mass deviation was 10 ppm and a setting of one and two peptide/proteins for kinase client assay peptide and autophosphorylated kinase were used, respectively, to further filter the data. For final validation, each spectrum was inspected manually and accepted only when the phosphopeptide had the highest pRS site probability, pRS score, XCorr value, and site-determining fragment ions allowed unambiguous localization of the phosphorylation site. Phosphopeptides with a pRS score $\geq$ 15 and/or a pRS site probability of $\geq$50% were accepted.

Functional Protein Microarray

Purified ILK1-V5 (9 μg) was used to probe both Arabidopsis protein chip 1 and 2 as described previously in Brauer et al. (2014) except the probing buffer contained 12.5 mM Tris pH 7 and 1% BSA. Chips were probed in triplicate and compared to three control chips where signal of the Cy5-conjugated anti-V5 antibody was quantified using a Scan Array Express (PerkinElmer, Waltham, MA).

Accession Numbers

Sequence data from this article can be found in the GenBank/EMBL data libraries under accession numbers At2g43850 (ILK1); At3g51920 (CML9); and At4g13420 (HAK5).

Supplemental Data

The following supplemental materials are available:

Supplemental Figure S1. Analysis of autophosphorylation sites in ILK1 in the presence of Mn^{2+} or Mg^{2+} cofactors.

Supplemental Figure S2. Relative purity of ILK1 isoforms used to conduct kinase assays.

Supplemental Figure S3. Bacterial growth is unaltered in *ilk1-1* knockdown line infected with *P. syringae* pv. *tomato* DC3000 or DC3000 AvrRpt2 strains.

Supplemental Table S1. Identification of phosphorylated serines in purified ILK1 and $ILK1^{D319N}$ protein using mass spectrometry.

Supplemental Table S2. The primer pairs used in this study.

Supplemental Table S3. Transporters identified as putative ILK1 phosphorylation targets and protein interaction targets using the KiC and functional protein microarrays (FPM).

Supplemental Data S1. Ionomic profile for flg22-treated seedlings.

ACKNOWLEDGMENTS

We gratefully acknowledge Austin Lee, Meeta Srivastava, and Mamta Srivastava for their assistance in conducting experiments; G. Popescu (The National Institute for Laser, Plasma & Radiation Physics) for contributions to formulating the ILK models; and A. Collmer (Cornell University), G. Martin (Boyce Thompson Institute), F. Rubio, J. Larkin (Louisiana State University), and N. Kumar (Louisiana State University) for providing biological reagents.

Received January 9, 2016; accepted April 29, 2016; published May 2, 2016.

LITERATURE CITED

Adams JA (2001) Kinetic and catalytic mechanisms of protein kinases. Chem Rev **101:** 2271–2290

Ahmed AU, Sarvestani ST, Gantier MP, Williams BRG, Hannigan GE (2014) Integrin-linked kinase modulates lipopolysaccharide- and *Helicobacter*

pylori-induced nuclear factor κB-activated tumor necrosis factor-α production via regulation of p65 serine 536 phosphorylation. J Biol Chem **289:** 27776–27793

Ahsan N, Huang Y, Tovar-Mendez A, Swatek KN, Zhang J, Miernyk JA, Xu D, Thelen JJ (2013) A versatile mass spectrometry-based method to both identify kinase client-relationships and characterize signaling network topology. J Proteome Res **12:** 937–948

Alemán F, Nieves-Cordones M, Martínez V, Rubio F (2011) Root K^+ acquisition in plants: the *Arabidopsis thaliana* model. Plant Cell Physiol **52:** 1603–1612

Arlehamn CSL, Pétrilli V, Gross O, Tschopp J, Evans TJ (2010) The role of potassium in inflammasome activation by bacteria. J Biol Chem **285:** 10508–10518

Atkinson, MM, Baker C (1987) Alteration of plasmalemma sucrose transport in *Phaseolus vulgaris* by *Pseudomonas syringae* pv. syringae and its association with K^+/H^+ exchange. Phytopathology **77:** 1573–1574

Boller T, Felix G (2009) A renaissance of elicitors: perception of microbe-associated molecular patterns and danger signals by pattern-recognition receptors. Annu Rev Plant Biol **60:** 379–406

Boudsocq M, Willmann MR, McCormack M, Lee H, Shan L, He P, Bush J, Cheng S-H, Sheen J (2010) Differential innate immune signalling via Ca^{2+} sensor protein kinases. Nature **464:** 418–422

Brauer E, Popescu S, Popescu G (2014) Experimental and analytical approaches to characterize plant kinases using protein microarrays. *In* G Komis, J Šamaj, eds, Plant MAP Kinases SE-17. Springer, New York, pp 217–235

Chinchilla D, Frugier F, Raices M, Merchan F, Giammaria V, Gargantini P, Gonzalez-Rizzo S, Crespi M, Ulloa R (2008) A mutant ankyrin protein kinase from *Medicago sativa* affects *Arabidopsis* adventitious roots. Funct Plant Biol **35:** 92–101

Chinchilla D, Merchan F, Megias M, Kondorosi A, Sousa C, Crespi M (2003) Ankyrin protein kinases: a novel type of plant kinase gene whose expression is induced by osmotic stress in alfalfa. Plant Mol Biol **51:** 555–566

Chinchilla D, Zipfel C, Robatzek S, Kemmerling B, Nürnberger T, Jones JDG, Felix G, Boller T (2007) A flagellin-induced complex of the receptor FLS2 and BAK1 initiates plant defence. Nature **448:** 497–500

Colomar A, Marty V, Médina C, Combe C, Parnet P, Amédée T (2003) Maturation and release of interleukin-1β by lipopolysaccharide-primed mouse Schwann cells require the stimulation of P2X7 receptors. J Biol Chem **278:** 30732–30740

Davies E (1987) Action potentials as multifunctional signals in plants: a unifying hypothesis to explain apparently disparate wound responses. Plant Cell Environ **10:** 623–631

Demidchik V, Cuin TA, Svistunenko D, Smith SJ, Miller AJ, Shabala S, Sokolik A, Yurin V (2010) Arabidopsis root K^+-efflux conductance activated by hydroxyl radicals: single-channel properties, genetic basis and involvement in stress-induced cell death. J Cell Sci **123:** 1468–1479

Felle HH, Kondorosi É, Kondorosi Á, Schultze M (1998) The role of ion fluxes in Nod factor signalling in *Medicago sativa*. Plant J **13:** 455–463

Fu H-H, Luan S (1998) AtKuP1: a dual-affinity K^+ transporter from *Arabidopsis*. Plant Cell **10:** 63–73

Fujikawa Y, Kato N (2007) Split luciferase complementation assay to study protein-protein interactions in *Arabidopsis* protoplasts. Plant J **52:** 185–195

Gampala SS, Kim T-W, He J-X, Tang W, Deng Z, Bai M-Y, Guan S, Lalonde S, Sun Y, Gendron JM, Chen H, Shibagaki N, et al (2007) An essential role for 14-3-3 proteins in brassinosteroid signal transduction in *Arabidopsis*. Dev Cell **13:** 177–189

Gómez-Gómez L, Boller T (2000) FLS2: an LRR receptor-like kinase involved in the perception of the bacterial elicitor flagellin in *Arabidopsis*. Mol Cell **5:** 1003–1011

Gomord V, Denmat LA, Fitchette-Lainé AC, Satiat-Jeunemaitre B, Hawes C, Faye L (1997) The C-terminal HDEL sequence is sufficient for retention of secretory proteins in the endoplasmic reticulum (ER) but promotes vacuolar targeting of proteins that escape the ER. Plant J **11:** 313–325

Hannigan GE, McDonald PC, Walsh MP, Dedhar S (2011) Integrin-linked kinase: not so 'pseudo' after all. Oncogene **30:** 4375–4385

He Y, Zeng MY, Yang D, Motro B, Núñez G (2016) NEK7 is an essential mediator of NLRP3 activation downstream of potassium efflux. Nature **530:** 354–357

Held K, Pascaud F, Eckert C, Gajdanowicz P, Hashimoto K, Corratgé-Faillie C, Offenborn JN, Lacombe B, Dreyer I, Thibaud J-B, Kudla J (2011) Calcium-dependent modulation and plasma membrane targeting of the AKT2 potassium channel by the CBL4/CIPK6 calcium sensor/protein kinase complex. Cell Res **21:** 1116–1130

Ichimura K, Shinozaki K, Tena G, Sheen J, Henry Y, Champion A, Kreis M, Zhang S, Hirt H, Wilson C; MAPK Group (2002) Mitogen-activated protein kinase cascades in plants: a new nomenclature. Trends Plant Sci **7:** 301–308

Jabs T, Tschöpe M, Colling C, Hahlbrock K, Scheel D (1997) Elicitor-stimulated ion fluxes and O_{2-} from the oxidative burst are essential components in triggering defense gene activation and phytoalexin synthesis in parsley. Proc Natl Acad Sci USA **94:** 4800–4805

Jeworutzki E, Roelfsema MRG, Anschütz U, Krol E, Elzenga JTM, Felix G, Boller T, Hedrich R, Becker D (2010) Early signaling through the Arabidopsis pattern recognition receptors FLS2 and EFR involves Ca-associated opening of plasma membrane anion channels. Plant J **62:** 367–378

Jones AME, MacLean D, Studholme DJ, Serna-Sanz A, Andreasson E, Rathjen JP, Peck SC (2009) Phosphoproteomic analysis of nuclei-enriched fractions from *Arabidopsis thaliana*. J Proteomics **72:** 439–451

Kato N, Jones J (2010) The split luciferase complementation assay. Methods Mol Biol **655:** 359–376

Kilian J, Whitehead D, Horak J, Wanke D, Weinl S, Batistic O, D'Angelo C, Bornberg-Bauer E, Kudla J, Harter K (2007) The AtGenExpress global stress expression data set: protocols, evaluation and model data analysis of UV-B light, drought and cold stress responses. Plant J **50:** 347–363

Kolb AR, Needham PG, Rothenberg C, Guerriero CJ, Welling PA, Brodsky JL (2014) ESCRT regulates surface expression of the Kir2.1 potassium channel. Mol Biol Cell **25:** 276–289

Kuchitsu K, Yazaki Y, Sakano K, Shibuya N (1997) Transient cytoplasmic pH change and ion fluxes through the plasma membrane in suspension-cultured rice cells rriggered by N-acetylchitooligosaccharide elicitor. Plant Cell Physiol **38:** 1012–1018

Leba L-J, Cheval C, Ortiz-Martín I, Ranty B, Beuzón CR, Galaud J-P, Aldon D (2012a) CML9, an *Arabidopsis* calmodulin-like protein, contributes to plant innate immunity through a flagellin-dependent signalling pathway. Plant J **71:** 976–989

Leba L-J, Perochon A, Cheval C, Ranty B, Galaud J-P, Aldon D (2012b) CML9, a multifunctional *Arabidopsis thaliana* calmodulin-like protein involved in stress responses and plant growth? Plant Signal Behav **7:** 1121–1124

Lee HY, Bowen CH, Popescu GV, Kang H-G, Kato N, Ma S, Dinesh-Kumar S, Snyder M, Popescu SC (2011) *Arabidopsis* RTNLB1 and RTNLB2 Reticulon-like proteins regulate intracellular trafficking and activity of the FLS2 immune receptor. Plant Cell **23:** 3374–3391

Lee SC, Lan W-Z, Kim B-G, Li L, Cheong YH, Pandey GK, Lu G, Buchanan BB, Luan S (2007) A protein phosphorylation/dephosphorylation network regulates a plant potassium channel. Proc Natl Acad Sci USA **104:** 15959–15964

Li F, Wang J, Ma C, Zhao Y, Wang Y, Hasi A, Qi Z (2013) Glutamate receptor-like channel3.3 is involved in mediating glutathione-triggered cytosolic calcium transients, transcriptional changes, and innate immunity responses in *Arabidopsis*. Plant Physiol **162:** 1497–1509

Ligaba A, Dreyer I, Margaryan A, Schneider DJ, Kochian L, Piñeros M (2013) Functional, structural and phylogenetic analysis of domains underlying the Al sensitivity of the aluminum-activated malate/anion transporter, TaALMT1. Plant J **76:** 766–780

Lozano-Durán R, Zipfel C (2015) Trade-off between growth and immunity: role of brassinosteroids. Trends Plant Sci **20:** 12–19

Magnan F, Ranty B, Charpenteau M, Sotta B, Galaud JP, Aldon D (2008) Mutations in AtCML9, a calmodulin-like protein from *Arabidopsis thaliana*, alter plant responses to abiotic stress and abscisic acid. Plant J **56:** 575–589

Maron LG, Kirst M, Mao C, Milner MJ, Menossi M, Kochian LV (2008) Transcriptional profiling of aluminum toxicity and tolerance responses in maize roots. New Phytol **179:** 116–128

Maydan M, McDonald PC, Sanghera J, Yan J, Rallis C, Pinchin S, Hannigan GE, Foster LJ, Ish-Horowicz D, Walsh MP, Dedhar S (2010) Integrin-linked kinase is a functional Mn^{2+}-dependent protein kinase that regulates glycogen synthase kinase-3β (GSK-3β) phosphorylation. PLoS One **5:** e12356

Mithöfer A, Ebel J, Felle HH (2005) Cation fluxes cause plasma membrane depolarization involved in β-glucan elicitor-signaling in soybean roots. Mol Plant Microbe Interact **18:** 983–990

Moran N, Ehrenstein G, Iwasa K, Mischke C, Bare C, Satter RL (1988) Potassium channels in motor cells of *Samanea saman*; a patch-clamp study. Plant Physiol **88:** 643–648

Moreau M, Westlake T, Zampogna G, Popescu G, Tian M, Noutsos C, Popescu S (2013) The *Arabidopsis* oligopeptidases TOP1 and TOP2 are salicylic acid targets that modulate SA-mediated signaling and the immune response. Plant J **76:** 603–614

Nieves-Cordones M, Alemán F, Martínez V, Rubio F (2010) The *Arabidopsis thaliana* HAK5 K^+ transporter is required for plant growth and K^+ acquisition from low K^+ solutions under saline conditions. Mol Plant **3:** 326–333

Nour-Eldin HH, Hansen BG, Nørholm MHH, Jensen JK, Halkier BA (2006) Advancing uracil-excision based cloning towards an ideal technique for cloning PCR fragments. Nucleic Acids Res **34:** e122

Perregaux D, Gabel CA (1994) Interleukin-1β maturation and release in response to ATP and nigericin. Evidence that potassium depletion mediated by these agents is a necessary and common feature of their activity. J Biol Chem **269:** 15195–15203

Pétrilli V, Papin S, Dostert C, Mayor A, Martinon F, Tschopp J (2007) Activation of the NALP3 inflammasome is triggered by low intracellular potassium concentration. Cell Death Differ **14:** 1583–1589

Popescu SC, Popescu GV, Bachan S, Zhang Z, Seay M, Gerstein M, Snyder M, Dinesh-Kumar SP (2007) Differential binding of calmodulin-related proteins to their targets revealed through high-density *Arabidopsis* protein microarrays. Proc Natl Acad Sci USA **104:** 4730–4735

Qi Z, Hampton CR, Shin R, Barkla BJ, White PJ, Schachtman DP (2008) The high affinity K^+ transporter AtHAK5 plays a physiological role in planta at very low K^+ concentrations and provides a caesium uptake pathway in *Arabidopsis*. J Exp Bot **59:** 595–607

Qi Z, Stephens NR, Spalding EP (2006) Calcium entry mediated by GLR3.3, an *Arabidopsis* glutamate receptor with a broad agonist profile. Plant Physiol **142:** 963–971

Ragel P, Ródenas R, García-Martín E, Andrés Z, Villalta I, Nieves-Cordones M, Rivero RM, Martínez V, Pardo JM, Quintero FJ, Rubio F (2015) CIPK23 regulates HAK5-mediated high-affinity K^+ uptake in *Arabidopsis* roots. Plant Physiol **169:** 2863–2873

Rodríguez-Concepción M, Toledo-Ortiz G, Yalovsky S, Caldelari D, Gruissem W (2000) Carboxyl-methylation of prenylated calmodulin CaM53 is required for efficient plasma membrane targeting of the protein. Plant J **24:** 775–784

Rodríguez-Navarro A, Rubio F (2006) High-affinity potassium and sodium transport systems in plants. J Exp Bot **57:** 1149–1160

Rubio F, Alemán F, Nieves-Cordones M, Martínez V (2010) Studies on *Arabidopsis* athak5, atakt1 double mutants disclose the range of concentrations at which AtHAK5, AtAKT1 and unknown systems mediate K uptake. Physiol Plant **139:** 220–228

Rubio F, Fon M, Ródenas R, Nieves-Cordones M, Alemán F, Rivero RM, Martínez V (2014) A low K^+ signal is required for functional high-affinity K^+ uptake through HAK5 transporters. Physiol Plant **152:** 558–570

Rubio F, Rodríguez-Navarro A (2000) Cloning of *Arabidopsis* and barley cDNAs encoding HAK potassium transporters in root and shoot cells. Physiol Plant **109:** 34–43

Scheel O, Papavlassopoulos M, Blunck R, Gebert A, Hartung T, Zähringer U, Seydel U, Schromm AB (2006) Cell activation by ligands of the toll-like receptor and interleukin-1 receptor family depends on the function of the large-conductance potassium channel MaxiK in human macrophages. Infect Immun **74:** 4354–4356

Scherzer S, Böhm J, Krol E, Shabala L, Kreuzer I, Larisch C, Bemm F, Al-Rasheid KAS, Shabala S, Rennenberg H, Neher E, Hedrich R (2015) Calcium sensor kinase activates potassium uptake systems in gland cells of Venus flytraps. Proc Natl Acad Sci USA **112:** 7309–7314

Seydel U, Scheel O, Müller M, Brandenburg K, Blunck R (2001) A K^+ channel is involved in LPS signaling. J Endotoxin Res **7:** 243–247

Singh DK, Calviño M, Brauer EK, Fernandez-Pozo N, Strickler S, Yalamanchili R, Suzuki H, Aoki K, Shibata D, Stratmann JW, Popescu GV, Mueller LA, et al (2014) The tomato kinome and the tomato kinase library ORFeome: novel resources for the study of kinases and signal transduction in tomato and solanaceae species. Mol Plant Microbe Interact **27:** 7–17

Spalding EP, Hirsch RE, Lewis DR, Qi Z, Sussman MR, Lewis BD (1999) Potassium uptake supporting plant growth in the absence of AKT1 channel activity: inhibition by ammonium and stimulation by sodium. J Gen Physiol **113:** 909–918

Walev I, Reske K, Palmer M, Valeva A, Bhakdi S (1995) Potassium-inhibited processing of IL-1β in human monocytes. EMBO J **14:** 1607–1614

Wang Y, Wu W-H (2010) Plant sensing and signaling in response to K^+-deficiency. Mol Plant **3:** 280–287

Wendehenne D, Lamotte O, Frachisse J-M, Barbier-Brygoo H, Pugin A (2002) Nitrate efflux is an essential component of the cryptogein signaling pathway leading to defense responses and hypersensitive cell death in tobacco. Plant Cell **14:** 1937–1951

Wickström SA, Lange A, Montanez E, Fässler R (2010) The ILK/PINCH/parvin complex: the kinase is dead, long live the pseudokinase! EMBO J **29:** 281–291

Yamaguchi-Shinozaki K, Shinozaki K (1994) A novel cis-acting element in an *Arabidopsis* gene is involved in responsiveness to drought, low-temperature, or high-salt stress. Plant Cell **6:** 251–264

Zielinski RE (2002) Characterization of three new members of the *Arabidopsis thaliana* calmodulin gene family: conserved and highly diverged members of the gene family functionally complement a yeast calmodulin null. Planta **214:** 446–455

Zipfel C, Robatzek S, Navarro L, Oakeley EJ, Jones JDG, Felix G, Boller T (2004) Bacterial disease resistance in *Arabidopsis* through flagellin perception. Nature **428:** 764–767